EasyChair Preprint

№ 12983

Multi-Objective Optimization of the Large Telescope Backup Structure Under Wind Loading

Hiroaki Kawamura, Chihiro Imamura, Akio Taniguchi, Yoichi Tamura and Toshiaki Kimura

April 9, 2024

Proceedings of the IASS 2024 Symposium
Redefining the Art of Structural Design
August 26-30, 2024, Zurich Switzerland
Philippe Block, Giulia Boller, Catherine DeWolf,
Jacqueline Pauli, Walter Kaufmann (eds.)

Multi-objective optimization of the large telescope backup structure under wind loading

Hiroaki KAWAMURA*, Chihiro IMAMURA[a], Akio TANIGUCHI[a], Yoichi TAMURA[a], Toshiaki KIMURA[b]

*Graduate School of Design and Architecture, Nagoya City University
Kita-Chikusa, Chikusa-ku, Nagoya, Japan
kawamura@sda.nagoya-cu.ac.jp

[a] Graduate School of Science, Nagoya University
[b] Graduate School of Design and Architecture, Nagoya City University

Abstract

This paper describes a numerical design method for homologous deformation problems in large telescope structural design using heuristic optimization. The Large Submillimeter Telescope (LST), a new 50-meter class single-dish telescope, is planned to be constructed in Chile. From the view of the structural design of the LST, the primary reflector's lattice backup structure (BUS), which comprises lattice elements and joints, prefers to be lightweight because the surface accuracy of the primary reflector depends on self-weight deformation. Furthermore, BUS needs high stiffness to support its primary reflector because the surface accuracy requires an extremely small value to collect electromagnetic waves from deep space, regardless of its large diameter. In addition, various combinations of antenna posture and wind direction need to be considered because the LST antenna would be exposed to strong wind. Besides, the primary reflector should maintain a paraboloid shape against self-weight in various elevation angles and wind loads in various directions. In order to optimize homologous deformation performance, this paper uses multi-objective optimization. The proposed optimization procedure considers various loading conditions, such as wind directions and elevation angles of the antenna. Then, practical examples of the lattice structure of the LST model are demonstrated to show the effectiveness of the proposed solution.

Keywords: large submillimeter telescope, multi-objective optimization, spatial structures

1. Introduction

In an effort to increase the diameter of submillimeter telescopes to meet the scientific need for deep space exploration, the construction of a 50-m Large Submillimeter Telescope (LST) is planned as shown in Figure 1 (a) [1]. Because the Large Submillimeter Telescope requires high sensitivity and high-resolution optical performance, the support structure of the mirror surface should be lightweight and highly rigid. In addition, homologous deformation performance [2, 3], in which the mirror surface maintains a rotating paraboloidal plane after deformation under various loading conditions, is required for optical performance. The present paper describes a numerical method to design the LST structure using topology optimization considering its design requirements.

The large aperture of submillimeter-wave telescopes is necessary for performing an exploration with a large range and high resolution. The telescope's primary mirror is required to have a high mirror surface accuracy (e.g., less than 45 μm), and as the mirror surface becomes larger, the primary mirror should maintain accuracy even in a variety of observation postures. Figure 1 shows a conceptual diagram of the LST. The surface accuracy of the primary mirror is important for collecting electromagnetic waves from

deep space with high accuracy. Therefore, the backup structure (BUS) supporting the primary mirror must have high rigidity. Furthermore, the mirror surface accuracy requirement cannot be satisfied using ordinary building structure design methods; the allowable deformation of an ordinary large building is about 1/300 of its span, but if this is applied to a 50-m class large telescope, the maximum deflection would be 50 m/300 = 167 mm, which is extremely larger than mirror surface accuracy of 45 μm. Therefore, an optimal design that satisfies rigidity and mass performance is necessary. Although there are some examples of optimal design for improving the accuracy of the mirror surface in engineering telescopes with relatively small apertures, as shown in Figure 1 (b) [4], there are few studies on large radio telescopes with apertures in the 50-m class [5].

This paper presents a modified muti-objective optimization method considering wind loading. The design problem is formulated in Section 2. Then, a numerical simulation is conducted to validate the effectiveness of the proposed method in Section 3.

(a) (b)

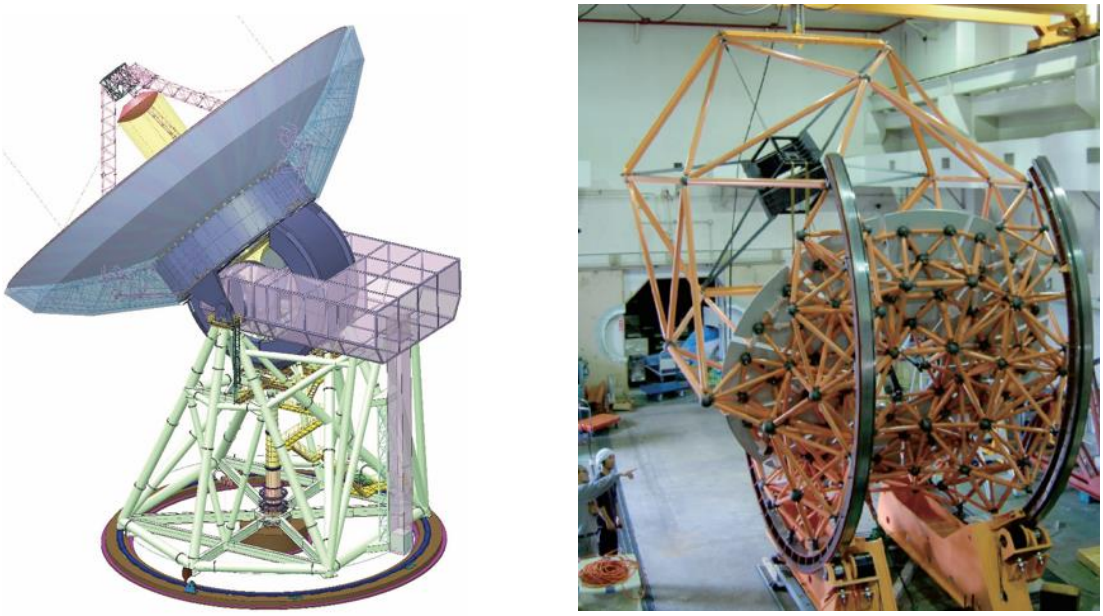

Figure 1. Examples of telescopes; (a) conceptual figure of LST [1], (b) heuristic-optimized BUS for 4 m class telescope [2]

2. Problem formulation

2.1. Linear elastic analysis

Figure 2 illustrates a cross-section image of a design domain for BUS and boundary condition with the elevation angle $\varphi \in [0, 90]$ equal to 90°. The design domain Ω is assumed to be consisted of n pieces of truss elements. Furthemore, whole deformation is assumed to be constrained on the surface of the hub domain Ω_h and Γ_D. On the reflector surface Γ_N, external loading on the reflector $\boldsymbol{f}$ and body forces of the BUS's self-weight $\boldsymbol{b}$ are applied. Truss elements in the domain Ω have the cross-sectional area, which is assigned as design variable $\boldsymbol{x} = (x_1, x_2, \dots, x_n)$. The cross-sectional area of i-th truss element x_i is selected from the material list $\boldsymbol{a}$, which consists of m kinds of standard dimension for each truss element. The solution set $\mathcal{D}$ is assigned as $\mathcal{D} = \{\boldsymbol{x} \in \boldsymbol{a} \mid \boldsymbol{a} = (a_1, a_2, \dots, a_m) \in \mathbb{R}^{n \times m}\}$. The BUS's displacement vector $\boldsymbol{u}$ are obtained by solving the equilibrium equation as follows:

$$\boldsymbol{K}(\boldsymbol{x})\boldsymbol{u} = \boldsymbol{f} + \boldsymbol{b}(\boldsymbol{x}), \tag{1}$$

where the global stiffness matrix represents $\boldsymbol{K}(\boldsymbol{x}) = \sum_{i=1}^{n} \boldsymbol{K}_i(x_i)$, with the element stiffness matrix $\boldsymbol{K}_i(x_i)$.

In this paper, the wind loading force f_{si} in part i of the reflector is expressed as follows:

$$f_{si} = \frac{1}{2}\rho\mu_{si}V_0^2 A_i, \tag{2}$$

where ρ, V_0, μ_{si} and A_i are air density, reference wind speed, shape function and pressure receiving area of the part i, respectively. The shape function μ_{si} depends on various factors (e.g., the location in the reflector, the aperture ratio, the elevation angle, the azimuth angle, etc). Generally, it can be estimated by various CFD analyses. However, to explore the applicability of the proposed method, the shape function in this paper is assigned according to the literature [6].

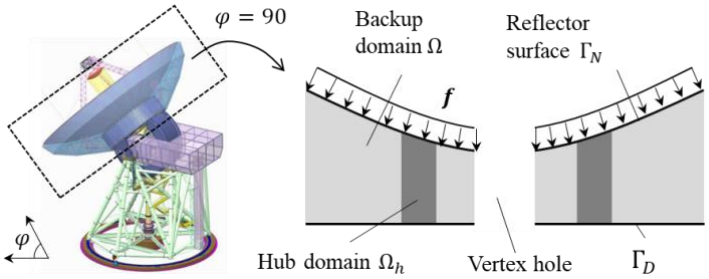

Figure 1: Cross-section image of the design domain of BUS and its boundary conditions with $\varphi = 90°$.

2.2. Homologous deformation of BUS

In designing the BUS, homologous deformation should be considered to keep a paraboloid shape after deformation to ensure the reflector accuracy of the telescope. Figure 2 illustrates the homologous deformation for the performance of the BUS. An undeformed reflector surface represents the ideal shape of the reflector surface without any deformation subjected to external loads. In contrast, a deformed reflector surface means the shape is deformed against external loads. The BUS can be allowed finite rigid displacement as long as the parabolic shape is maintained under given loading conditions. The elastically deformed shape needs to correspond to a target paraboloid shape. In this figure, the target paraboloid shape after deformation $\boldsymbol{S}(\boldsymbol{q}, \boldsymbol{p})$ is expressed by two parameters: the coordinates of the vertex $\boldsymbol{q}$ and focus $\boldsymbol{p}$, respectively. A certain range of variance of these parameters under several loading conditions is allowed because of the posture control of the secondary reflector that is located at the focus. Using the solution of Eq. (1)**,** the homologous deformation $h(\boldsymbol{u})$ can be evaluated as follows:

$$h(\boldsymbol{x}, \boldsymbol{u}) = \int_{\Gamma_N} (\boldsymbol{u}(\boldsymbol{x}) - \overline{\boldsymbol{u}}) \cdot (\boldsymbol{u}(\boldsymbol{x}) - \overline{\boldsymbol{u}})\, \mathrm{d}\Gamma_N, \tag{3}$$

where $\overline{\boldsymbol{u}}$ is the pre-described displacement vector defined on Γ_N. Note that $\overline{\boldsymbol{u}}$ can vary through the optimization process in this method. It can be defined as follows:

$$\overline{\boldsymbol{u}} = \boldsymbol{S}_0 - \boldsymbol{S}(\boldsymbol{q}, \boldsymbol{p}), \tag{4}$$

where $\boldsymbol{S}_0$ is the vector of the nodal coordinate of the surface of the undeformed primary reflector. $\boldsymbol{S}(\boldsymbol{q},\boldsymbol{p})$ is the target paraboloid shape vector with the given vertex coordinate of the primary reflector $\boldsymbol{q} = (q_x, q_y, q_z)^{\mathrm{T}}$ and the coordination of the focus point $\boldsymbol{p} = (p_x, p_y, p_z)^{\mathrm{T}}$. These parameters $\boldsymbol{q},\boldsymbol{p}$ used in Eq. (4) can be obtained by solving the following optimization problem:

$$\boldsymbol{d}(\boldsymbol{q},\boldsymbol{p}) = |\boldsymbol{u}(\boldsymbol{x}) + \boldsymbol{S}_0 - \boldsymbol{S}(\boldsymbol{q},\boldsymbol{p})|^2, \tag{5}$$

$$\boldsymbol{q},\boldsymbol{p} = \underset{\boldsymbol{x},\boldsymbol{y}}{\operatorname{argmin}} \int_{\Gamma_N} \boldsymbol{d}(\boldsymbol{x},\boldsymbol{y}) d\Gamma_N. \tag{6}$$

Eq (5) indicates the squared error vector of the homologous deformation.

Using the homologous deformation $h_\varphi(\boldsymbol{u},\boldsymbol{t},\boldsymbol{b})$ with loading condition $\boldsymbol{t}$ on the boundary Γ_t and body force $\boldsymbol{b} = \boldsymbol{b}(\boldsymbol{x})$ in the design domain Ω, we defined an objective function as follows:

$$J_\varphi = \int_t \boldsymbol{w}_\varphi(t) \cdot h_\varphi(\boldsymbol{u}, t, \boldsymbol{b}) dt \tag{7}$$

where, $\varphi \in [\varphi_{\min}, \varphi_{\max}]$ is the elevation angle of the reflector and $w_\varphi(t)$ is weight function to the loading condition $\boldsymbol{t}$ at the elevation angle φ. The stresses of truss elements with j-th cross-sectional area in the list are constrained using following function:

$$J_{t,i}(\boldsymbol{x}) = \prod_j^i \max\left(1, \frac{\sigma_{t,j}}{c_i}\right) \tag{8}$$

where, c_i represents constant upper value of the elemental stress of i-th element, and $\sigma_{t,i}$ indicates elemental stress of the j-th truss element under loading condition t. The optimization problem to minimize the objective function Eq. (6) while satisfying subjective functions Eq. (7) can be described as follows:

$$\min_{\boldsymbol{x}\in X}\{J_\varphi(\boldsymbol{u}) \mid J_{t,i}(\boldsymbol{x}) \le 0, i \in \{1,\dots,m\}, \boldsymbol{K}(\boldsymbol{x})\boldsymbol{u} = \boldsymbol{f}_t\}. \tag{9}$$

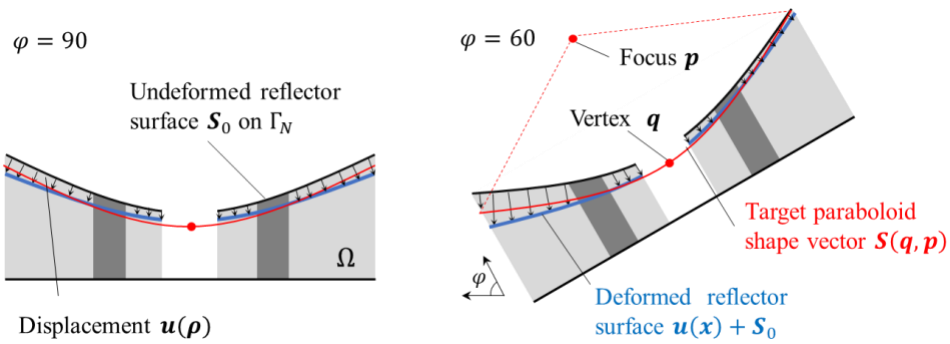

Figure 2: Homologous deformation for the performance of the primary reflector.

3. Numerical examples

3.1. Estimation of wind loading conditions

The distribution of wind loads acting on each part of the reflector depends on the part within the reflector surface, the elevation angle, and the direction of the wind relative to the reflector. Wind pressure is assumed to act uniformly on 20 regions divided according to Ref. [6]. Figure 3 illustrates an example of the regional divisions of the reflector surface. The direction of the wind relative to the reflector surface is assumed to be the direction shown in Figure 5. The red and blue-colored regions represent positive and negative pressure against the reflector surface, respectively.

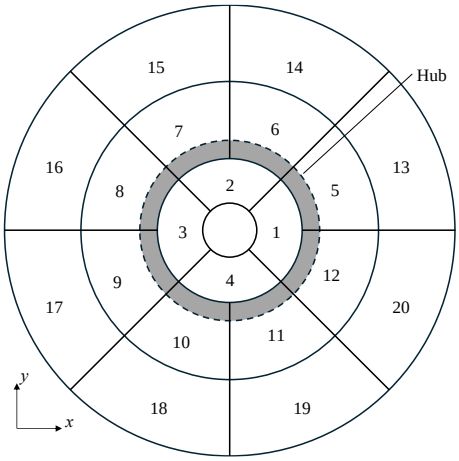

Figure 3: Regional division of the telescope surface S_0.

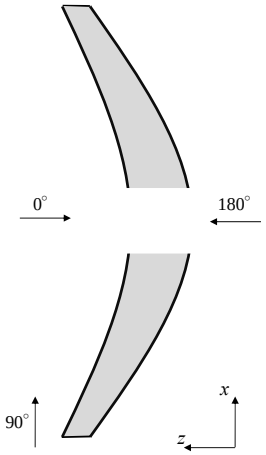

Figure 4: Wind direction.

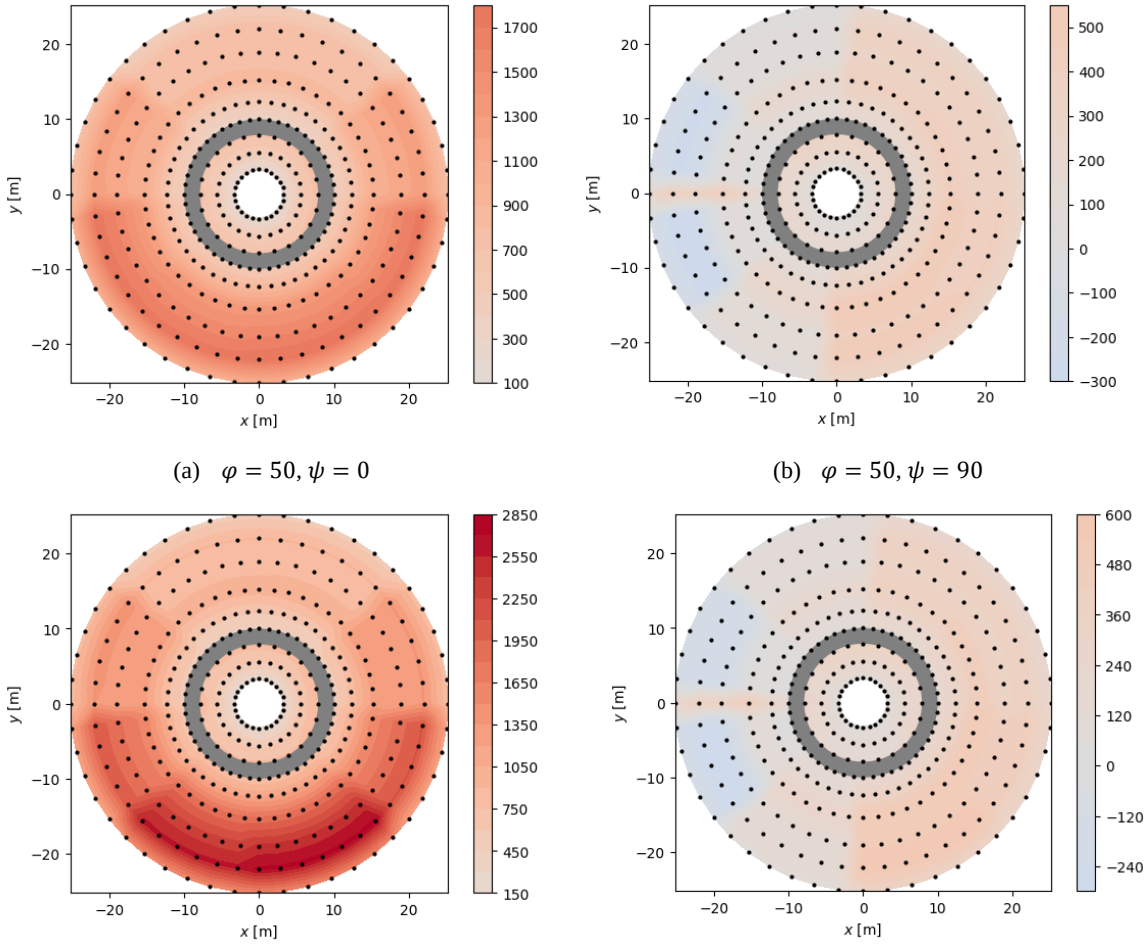

(a) $\varphi = 50, \psi = 0$ (b) $\varphi = 50, \psi = 90$

(c) $\varphi = 30, \psi = 0$ (d) $\varphi = 30, \psi = 90$

Figure 5: Nodal wind force distribution for each elevation angle φ and wind direction ψ.

3.2. Muti-objective optimization of BUS

The loading conditions shown in Table 1 are given to the BUS, and multi-objective optimization is performed for all loading conditions. As for computing the wind loads, the atmospheric density and the wind speed are set to $\rho = 0.976$ kg/m^3 and $V_0 = 15$ m/s, respectively. Table 2 shows optimization parameters. DEAP, which is the Python library for the genetic algorithm, is used for solving the optimization problem [7]. NSGA-II is selected for multi-objective optimization [8]. As for the linear static analysis, OpenSees is used to obtain the displacement for computing the homologous deformation performance of each solution [9].

Table 1: Loading cases

Case	Loading type	Elevation angle φ (deg.)	Wind direction ψ (deg.)
1	Gravity	85	-
2	Gravity	30	-
3	Gravity + wind	50	0
4	Gravity + wind	50	90
5	Gravity + wind	30	0
6	Gravity + wind	30	90

Table 2: Optimization parameters

Number of individuals	300
Number of generations	1000
Type of crossover	Two-point crossover
Crossover rate	0.9
Mutation rate	0.1
Selection algorithm	NSGA-II

Figure 6 shows the error distributions of homologous deformation evaluated using Eqs. (5) and (6) in terms of each loading condition. As seen in Figure 6, each error distribution corresponds to the elevation angles and wind directions. It can be seen that the error distribution under wind loading conditions is not negligible compared to the deformation due to dead weight. Furthermore, The results with consideration of wind loading, such as Case 3−Case 6, show that the maximum error value can be seen at the end of the surface. The optimal solution indicates that the outside of the surface needs to be reinforced for suitable deformation in the practical design.

4. Conclusion

This paper describes a multi-objective BUS optimization method for the LST, considering wind loading conditions. Numerical examples indicate the various error distributions corresponding to the elevation angle and wind direction. The optimal solution represents the effectiveness of the proposed method.

References

[1] R. Kawabe, K. Kohno, Y. Tamura, T. Takekoshi, T. Oshima, and S. Ishii, “New 50-m-class single-dish telescope; Large Submillimeter Telescope (LST)” Proceedings of SPIE, vol. 9906, 2016. https://doi.org/10.1117/12.2232202

[2] S. V. Hoerner, Homologous Deformation of Tiltable Telescope, Proceedings of the American Society of Civil Engineers, Journal of the Structural Division, 93 (5), 1967

[3] Y., Hangai, Shape Analysis of Structures, Theoretical and Applied Mechanics, vol. 39, Proceedings of 39th Japan National Congress for Applied Mechanics, Ed. JNCTAM, Science Council of Japan, University of Tokyo Press, 1990.

[4] M. Kunda, M. Kurita, and H. Ohmori, “Computational Morphogenesis of Truss Structures – Application to Telescope Structure –”, Journal of the International Association for Shell and Spatial Structures, vol. 53, 1, 171, pp. 49-56 (8), 2012.

[5] H.Kawamura, et al., “Multi-objective optimization of the large telescope structure under temperature loading.” Proceedings of IASS Anual Symposium, 1443-1450, 2023

[6] Yan Liu, Hong-liang Qian and Feng Fan, “Reflector wind load characteristics of the large all-movable antenna and its effect of reflector surface precision”, Advanced Steel Construction, vol. 13, no. 1, pp. 1-29, 2017

[7] Fortin, F.-A. et al., DEAP: Evolutionary algorithms made easy. Journal of Machine Learning Research, 13, p.2171–2175, 2012.

[8] Deb, K., Pratap, A., Agarwal, S., and Meyarivan, T. “A fast and elitist multiobjective genetic algorithm: NSGA-II,” IEEE Transactions on Evolutionary Computation 6, No. 2, 182-197, 2002, DOI: 10.1109/4235.996017.

[9] https://opensees.berkeley.edu

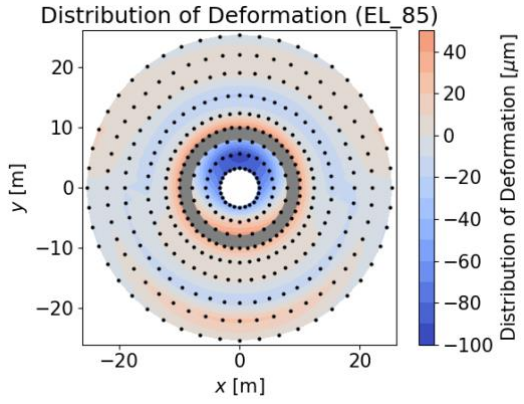

(a) Case 1: $\varphi = 85$

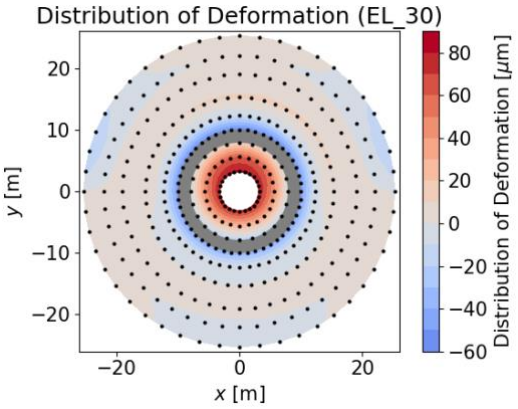

(b) Case 2: $\varphi = 30$

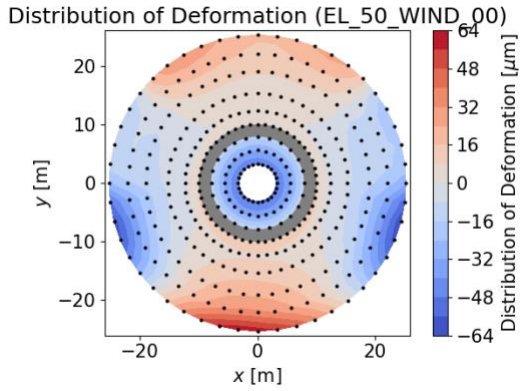

(c) Case 3: $\varphi = 50, \psi = 0$

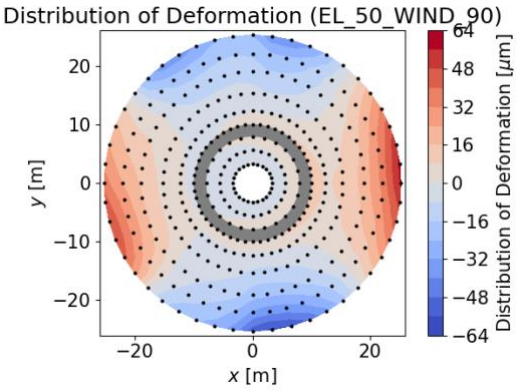

(d) Case 4: $\varphi = 50, \psi = 90$

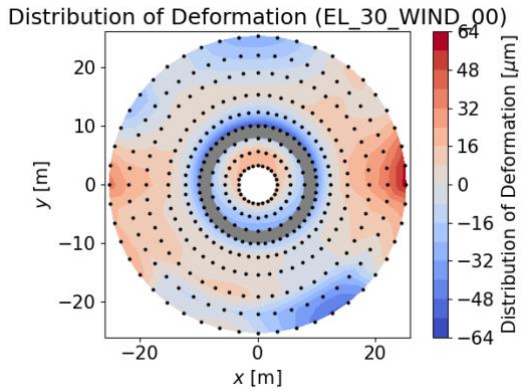

(e) Case 5: $\varphi = 30, \psi = 0$

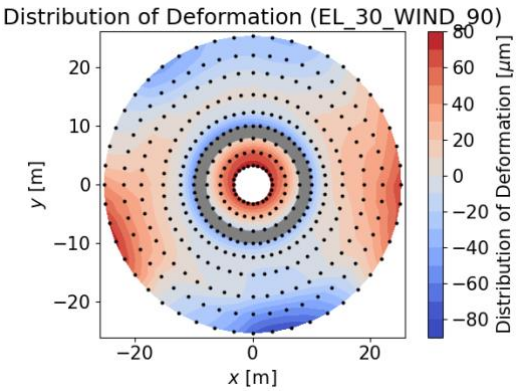

(f) Case 6: $\varphi = 30, \psi = 90$

Figure 6: Error distributions of homologous deformation estimated using Eq. (5).